J. Jpn. Soc. Powder Powder Metallurgy, **69** (2022) 461-466
https://doi.org/10.2497/jjspm.69.461

Paper

Study on Site Preference and Electronic State of $Y_2(Mn_xFe_{1-x})_{12}P_7$ with the $Zr_2Fe_{12}P_7$-type Structure

Taiki SHIOTANI[1]*, Hiroto OHTA[2], Takeshi WAKI[1], Yoshikazu TABATA[1] and Hiroyuki NAKAMURA[1]

[1]Department of Materials Science and Engineering, Kyoto University, Sakyo-ku, Kyoto 606-8501, Japan.
[2]Department of Molecular Chemistry and Biochemistry, Faculty of Science and Engineering, Doshisha University, Kyotanabe 610-0321, Japan.

Received March 14, 2022; Accepted April 21, 2022

ABSTRACT

We studied a solid-solution system of the transition-metal pnictide, $Y_2(Mn_xFe_{1-x})_{12}P_7$, with the $Zr_2Fe_{12}P_7$-type structure, which has two kinds of transition metal sites: three tetrahedral sites and a pyramidal site. We successfully obtained polycrystalline samples of $Y_2(Mn_xFe_{1-x})_{12}P_7$ in the range of $0 \leqq x \leqq 0.9$. The lattice parameter along the *a*-axis monotonically increases with the Mn substitution, while that along the *c*-axis is nearly constant. ^{57}Fe Mössbauer spectroscopy shows that Mn atoms prefer to occupy the pyramidal site. At $x = 0.25$, the site-ordered compound, $Y_2Mn_3Fe_9P_7$, was obtained, where Mn atoms occupy the pyramidal site and Fe atoms occupy the tetrahedral sites. The magnetization of $Y_2Mn_3Fe_9P_7$ exhibits an anomaly at approximately 60 K, suggesting presence of an antiferromagnetic transition, which originates from the magnetic moment of Mn at the pyramidal site.

KEY WORDS

$Y_2(Mn_xFe_{1-x})_{12}P_7$, itinerant magnetism, site preference, $Zr_2Fe_{12}P_7$-type structure

1 Introduction

Transition-metal pnictides with *TmPn* layers, where *Tm* and *Pn* stand for the transition-metal and pnictogen atoms, respectively, have attracted much attention since discovering a superconductivity in $LaFeAs(O_{1-x}F_x)$[1)]. The *TmPn* layer consisting of edge-shared $TmPn_4$ tetrahedrons has been studied intensively as a two-dimensional strongly correlated electron system of itinerant 3*d* electrons belonging to *Tm*. The electronic properties vary significantly by *Tm*: in the case of *Pn* = P, Pauli paramagnetism and superconductivity with a low critical temperature for *Tm* = Fe and Ni[2,3)], and itinerant electron ferromagnetism for *Tm* = Co[4)].

Many transition-metal pnictides include the $TmPn_4$ tetrahedrons. Among them, pnictides with the atomic ratio of metal (lanthanoids and transition metals) to pnictogen, 2:1, mainly consist of the $TmPn_4$ tetrahedrons and five-coordinated $TmPn_5$ pyramids. Typical examples are compounds with the Fe_2P-type structure such as Fe_2P and Mn_2P. The Fe_2P-type structure is the first member of homologous series with the general formula, $RE_{n(n-1)}Tm_{(n+1)(n+2)}Pn_{n(n+1)+1}$ (*RE*: group 3 and 4, *n* = 1, 2, 3...), and the second member is the $Zr_2Fe_{12}P_7$-type structure. The $Zr_2Fe_{12}P_7$-type structure is closely related to layered pnictides with the *TmPn* layers. Fig. 1 shows the structure of $Y_2Tm_{12}P_7$ (*Tm* = Mn, Fe, Co, Ni) having the $Zr_2Fe_{12}P_7$-type structure. It crystallizes in a hexagonal structure with the space group $P\bar{6}$ (No. 174)[6)]. Three of four crystallographic *Tm* sites are tetrahedrally coordinated forming the TmP_4 tetrahedrons. These tetrahedrons share edges to form a three-leg ladder (Fig. 1 (b)). This structure is a narrow-strip version of the *TmPn* layer, and thus the 3*d* electrons of *Tm* travel around in the ladder. $Y_2Tm_{12}P_7$, therefore, exhibits the same electronic properties as corresponding layered pnictides with the *TmPn* layer; for example, $Y_2Co_{12}P_7$ is an itinerant electron ferromagnet (T_C ~ 150 K)[7)] as well as LaCoPO, and in the case of *Tm* = Fe and Ni, $Y_2Tm_{12}P_7$ is Pauli paramagnetic[8,9)] similarly to LaFePO and LaNiPO. The last one of the four *Tm* sites is a pyramidal site forming the TmP_5 pyramids, which share edges of the base rectangle to form a linear chain along the *c* axis (Fig. 1 (c)). Two Y sites are surrounded by six P atoms to form YP_6 trigonal prisms and share the top and bottom faces to form a linear chain along the *c* axis (Fig. 1 (d)). These chains and ladders are connected in the way shown in Fig. 1 (a).

As mentioned above, transition metals occupy two kinds of sites in the $Zr_2Fe_{12}P_7$-type structure: the tetrahedral sites and the pyramidal site. Dhahri pointed out that two different transition metals occupy these sites selectively in the case of a solid-solution system[10)]. According to the literature, a larger atom tends to occupy the pyramidal site and vice versa. The site-ordered compounds, $RE_2Mn_3Cu_9P_7$, have been reported[11)], where Mn atoms occupy the pyramidal site and Cu atoms occupy the tetrahedral sites. Recently, Kato *et al.* have reported the synthesis and physical properties

---

* Corresponding author, E-mail: shiotani.taiki48e@st.kyoto-ac.jp

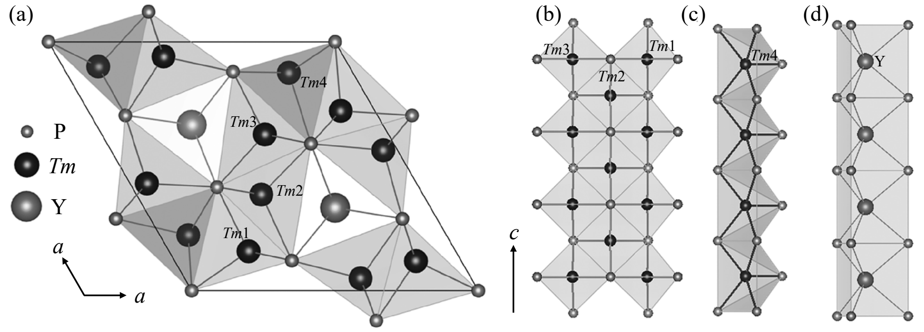

Fig. 1 (a) Crystal syructure of $Y_2Tm_{12}P_7$ (b) TmP_4 three-leg ladder (c) TmP_5 pyramid chain and (d) YP_6 trigonal prism chain drawn by VESTA.[5)]

of $Y_2Tm'_3Co_9P_7$ (Tm': transition metals)[12)]. In this system, the 3d electrons of Co at the tetrahedral sites are the origin of the itinerant electron ferromagnetism, whereas those at the pyramidal site are relatively localized and closely related to the stability of the ferromagnetic state. The nature of the 3d electrons at the pyramidal site is interesting but is not well understood. To investigate the problem, it is important to know how transition-metal atoms occupy the two kinds of sites. In the case of the Fe_2P-type structure, a lot of studies have been reported for the site preference of transition-metal atoms. Among them, in the Fe_2P-Mn_2P solid-solution system, Mn and Fe atoms show a strong site preference[13)]. In systems containing Fe atoms, the site preference of transition-metal atoms is well studied since ^{57}Fe Mössbauer spectroscopy is an excellent probe to determine the site occupancy of Fe atoms. As above, a solid-solution system, $Y_2(Mn_xFe_{1-x})_{12}P_7$, is ideal for studying the site preference in the $Zr_2Fe_{12}P_7$-type structure.

We report the results of synthesis, structure refinement, and ^{57}Fe Mössbauer spectroscopy of the $Y_2(Mn_xFe_{1-x})_{12}P_7$ solid-solution system. We discuss the site preference of Mn and Fe atoms in the $Zr_2Fe_{12}P_7$-type structure. We also report the results of the magnetization measurements and density functional theory calculations for the site-ordered $Y_2Mn_3Fe_9P_7$ and discuss the electronic state at the pyramidal site.

2 Experiments

Polycrystalline samples of $Y_2(Mn_xFe_{1-x})_{12}P_7$ were synthesized by a solid-state reaction. Powders of Y (Rare Metallic, purity: 99.9%), Mn (Rare Metallic, 99.95%), Fe (Rare Metallic, 99.9%) and P (Rare Metallic, 99.9999%) were used as starting materials. In the case of $x = 0.25$–1, the mixtures of these powders with an appropriately nominal ratio were heated at 1073 K for 3 h in an argon-filled silica tube. The obtained sample was well crushed and heated at 1373 K for 12 h in an argon-filled silica tube. For $x = 0$–0.25, YFe_2 was used as a precursor instead of Y and Fe powders. YFe_2 was synthesized by heating a mixture of Y and Fe powders with the stoichiometry ratio at 1073 K for 3 h in an argon-filled silica tube. The precursor was crushed and mixed with Fe, Mn and P powders with an appropriately nominal ratio. The heat treatment was the same as above.

The samples were characterized by powder X-ray diffraction (XRD) measurements using X'Pert PRO Alpha-1 (PANalytical) with Cu $K\alpha_1$ radiation. The structure refinement was carried out for the samples using Rietan-FP[14)].

The ^{57}Fe Mössbauer spectroscopy measurements were conducted in a conventional transmission geometry using ^{57}Co-in-Rh γ-ray source. The Doppler velocity scale was calibrated with respect to Fe-metal foil.

The magnetization (M) of the samples were measured in a SQUID magnetometer (MPMS, Quantum Design), equipped in Research Center for Low Temperature and Materials Science, Kyoto University, in the temperature range of 2–300 K at magnetic field of 10 kOe.

We calculated the electronic structure of $Y_2Mn_3Fe_9P_7$ by the full-potential linear augmented plane wave (FP-LAPW) method with the local density approximation (LDA) using the Perdew-Burker-Ernzerhof (PBE) exchange-correlation functional in the generalized gradient approximation (GGA) using the WIEN2k program package[15)].

3 Results and discussion

Fig. 2 shows powder XRD patterns of the prepared samples. $Y_2(Mn_xFe_{1-x})_{12}P_7$ were obtained as the main phase in the range of $x = 0$–0.9. These samples contain secondary phases such as $(Mn, Fe)_2P$ and $(Mn, Fe)_3P$. On the other hand, the XRD pattern of $x = 1.0$ is not of $Y_2Mn_{12}P_7$ but a superposition of those of YP, Mn_2P and Mn_3P. The peaks of $Y_2(Mn_xFe_{1-x})_{12}P_7$ shift towards a lower angle as x increased, indicating expansion of the unit-cell volume with x. We refined the structure parameters by the Rietveld analysis of the XRD patterns. Fig. 2 (b) shows an example of the results. Because the number of electrons at Mn is nearly equal to that at Fe, it is not easy to distinguish Mn and Fe in the analysis. We, therefore, firstly refined lattice parameters. Atomic positions were refined after considering the results of Mössbauer spectroscopy. Fig. 3 shows the x dependence of the lattice parameters a, c and the unit-cell volume V. The c is nearly constant with x, while the a and V increase monotonically with x. The 90% Mn-substitution results in 7% expansion in the cell volume from the non-substituted case. These structural changes are similar to the case of $(Fe, Mn)_2P$

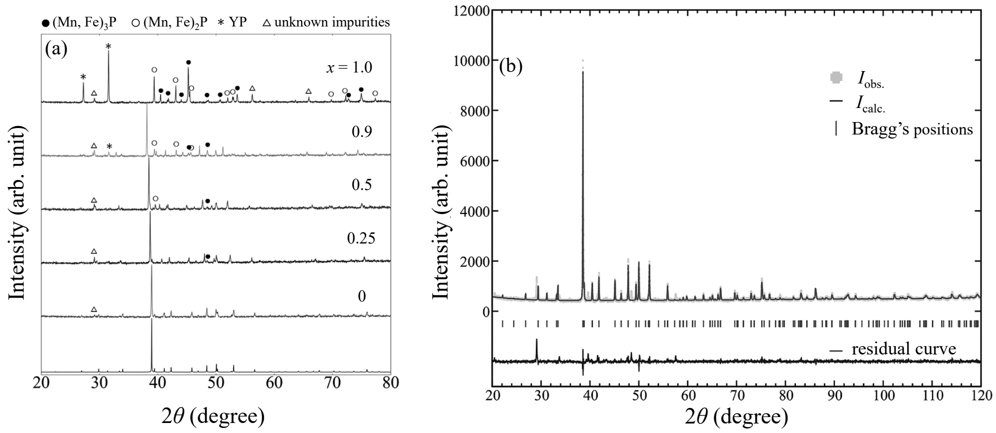

Fig. 2 (a) XRD patterns of $Y_2(Mn_xFe_{1-x})_{12}P_7$. (b) XRD pattern of $Y_2(Mn_{0.4}Fe_{0.6})_{12}P_7$ with the result of Rietveld refinement.

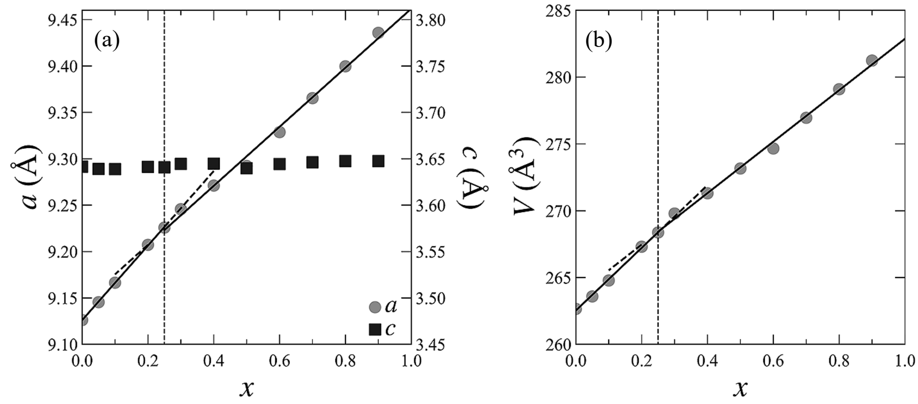

Fig. 3 (a) Lattice parameters a and c and (b) unit-cell volumes V of $Y_2(Mn_xFe_{1-x})_{12}P_7$.

solid-solution system[16]. These analyses show that the polyhedron of Mn is larger than that of Fe at both sites. As mentioned above, the *Tm′* substitution for *Tm* occurs at the pyramidal site selectively when the radius of *Tm′* is larger than that of *Tm*. In such a case, as increasing *Tm′* content, x, lattice parameters are expected to change their x dependences at $x = 0.25$ if *Tm′* ideally fills the pyramidal site. As shown in Fig. 3, the slope in a and V changed slightly, suggesting the preference of Mn to the pyramidal site.

We measured ^{57}Fe Mössbauer spectra of $Y_2(Mn_xFe_{1-x})_{12}P_7$ (x = 0–0.4) at room temperature to investigate the site occupation of the Mn and Fe atoms. Fig. 4 shows the transmission spectra. For $x = 0$, there are two peaks in the spectrum. This spectrum can be separated into two components assigned to the tetrahedral and pyramidal sites[8]. A Mössbauer spectrum shows a quadrupole splitting depending on the magnitude of electric field gradient (EFG). Here, the magnitude of the EFG at the Fe nuclei closely relates to the symmetry of the phosphorus polyhedron. Therefore, the quadrupole splitting should be small for the tetrahedral sites, while much larger for the pyramidal site. We analyzed the spectrum of $x = 0$ by fitting them to two Lorentz function pairs (double Lorentz function, DLFs) with equal height and width in each DLF. Fig. 4 shows the fitting result for $x = 0$ and the two DLFs simulated from the refined parameters. The area of the two DLFs, which correspond to the population of Fe atoms at the two sites, should be in the ratio in the number of atoms at the tetrahedral sites to the pyramidal site, 3:1, for $x = 0$. The experimental result agrees with the expectation. We obtained such a result, indicating the validity of our analysis. We show the fitting results for other x values in Fig. 4. Fig. 5 shows the occupancy (S) of the Mn atoms at the pyramidal site estimated from the analyses. For $x < 0.25$, S exhibits a linear increase with x, and for $x \geqq 0.25$, S is 1. This result indicates that Mn and Fe have a strong site preference for the pyramidal site and the tetrahedral sites, respectively, as in the case of $(Mn, Fe)_2P$. At $x = 0.25$, Mn and Fe occupy selectively the pyramidal site and the tetrahedral sites, respectively, implying that $Y_2(Mn_{0.25}Fe_{0.75})_{12}P_7$ can be regarded as the ordered compound, $Y_2Mn_3Fe_9P_7$. In Fig. 4, there is no splitting into six peaks, meaning that $Y_2(Mn_xFe_{1-x})_{12}P_7$ (x = 0–0.4) is in a paramagnetic state at room temperature.

Fig. 6 shows the x dependence of the isomer shift (I.S.) and the quadrupole splitting (Q.S.) obtained from the spectrum analyses. The I.S. and Q.S. are constant with x, suggesting that the electronic states of Fe at both sites are not modified by the Mn substitution. The I.S. of the tetrahedral sites is nearly equal to that of compounds with the FeP layer such as *Ae*Fe_2P_2 (*Ae* = Ca, Sr, Ba)[17]. Therefore, the electronic state of the FeP_4 tetrahedron in $Y_2(Mn_xFe_{1-x})_{12}P_7$ is likely to be Pauli paramagnetic as in the case of *Ae*Fe_2P_2. On the

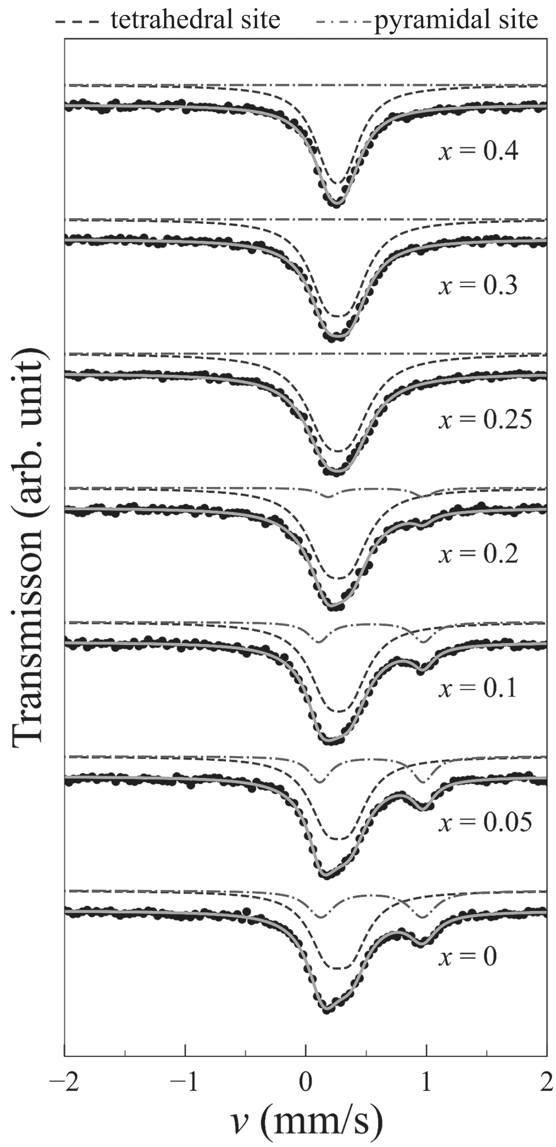

Fig. 4 ^{57}Fe Mössbauer spectra of $Y_2(Mn_xFe_{1-x})_{12}P_7$ (x = 0–0.4) at room temperature. Broken and dashed curves represent simulations for the tetrahedral-site and the pyramidal-site components, respectively.

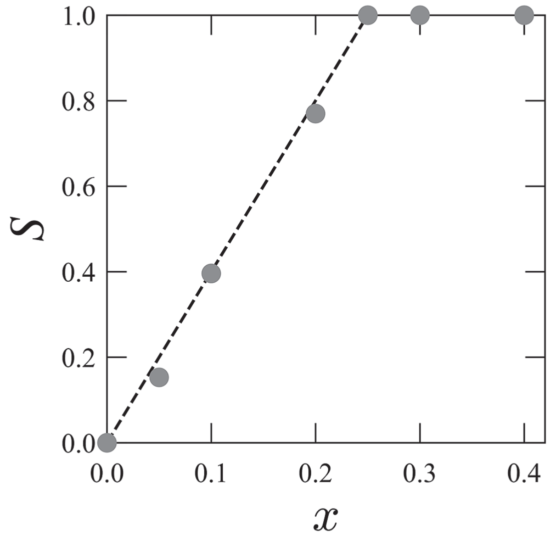

Fig. 5 Pyramidal site occupancy of Mn in $Y_2(Mn_xFe_{1-x})_{12}P_7$.

other hand, the I.S. of the pyramidal site is larger than that of the tetrahedral sites. Larger I.S. corresponds to lower *s* electron density at the Fe nuclear site. Thus, Fe at the pyramidal site is more ionic than that at the tetrahedral sites.

The results of Mössbauer spectroscopy reveal that Fe at the pyramidal site is rather ionic, and thus it is considered to have a rather stable magnetic moment. On the other hand, $Y_2Fe_{12}P_7$ is Pauli paramagnetic[8], suggesting that $Y_2Fe_{12}P_7$ has no magnetic moment. $Y_2Mn_3Fe_9P_7$ is a key material to resolve such a discrepancy and understand the electronic state of Fe in $Y_2Fe_{12}P_7$. Fig. 7 shows the temperature dependence of the magnetization of $Y_2Mn_3Fe_9P_7$. The magnetization exhibits an anomaly at approximately 60 K, indicating the presence of an antiferromagnetic transition. A similar anomaly has preliminarily been observed at around 40 K in $Y_2Mn_3Ni_9P_7$. In this compound, Mn at the pyramidal site solely possesses a magnetic moment, and thus the anomaly at 40 K is due to magnetic ordering in the Mn sublattice. In the present case, Mn is expected to possess a magnetic moment as in the case of the $Y_2Mn_3Ni_9P_7$. Thus, Fig. 7 indicates that the antiferromagnetic

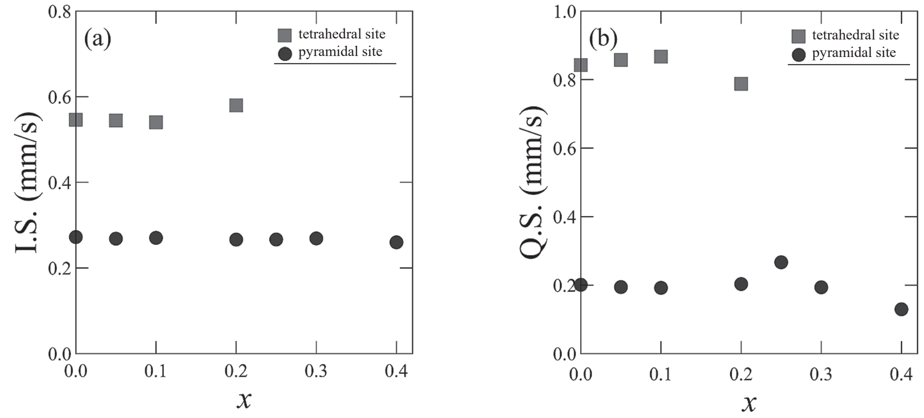

Fig. 6 (a) Isomer shift (I.S.) and (b) quadrupole splitting (Q.S.) of $Y_2(Mn_xFe_{1-x})_{12}P_7$ plotted against x. Circles are for the tetrahedral sites and squares for the pyramidal site.

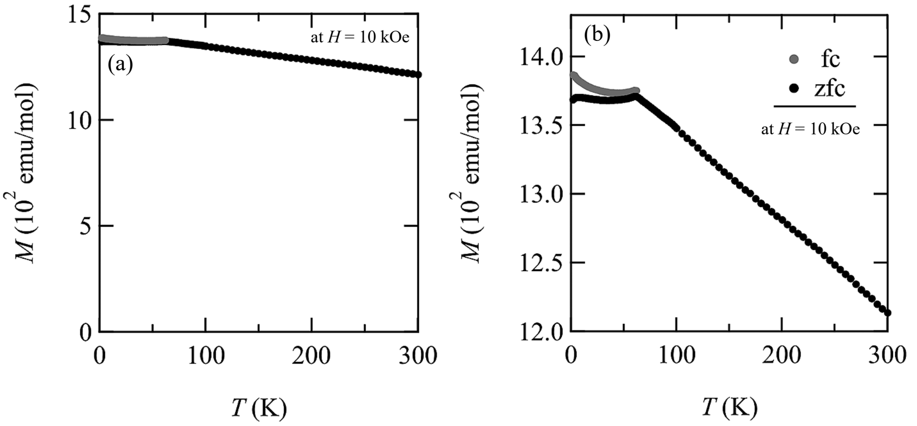

Fig. 7 Temperature dependences of the magnetization of $Y_2Mn_3Fe_9P_7$ at H = 10 kOe. (b) Magnification of panel (a) along the longitudinal axis.

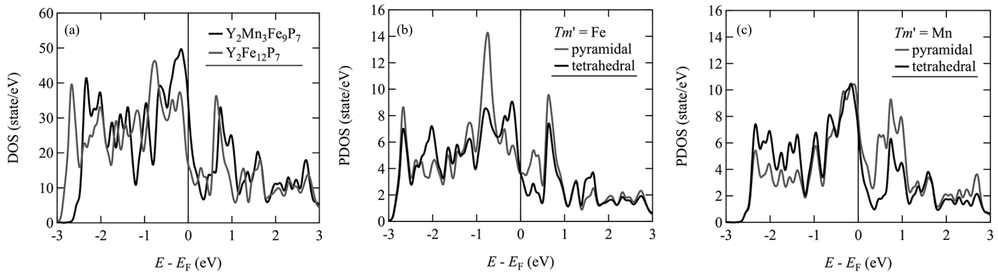

Fig. 8 (a) DOS of $Y_2Fe_{12}P_7$ and $Y_2Mn_3Fe_9P_7$, (b) PDOS of $Y_2Fe_{12}P_7$ and (c) PDOS of $Y_2Mn_3Fe_9P_7$.

state is realized in the sublattice of the pyramidal site below approximately 60 K. The inverse magnetic susceptibility exhibits a linear behavior against temperature in the paramagnetic region. The estimated effective Bohr magneton and the Weiss temperature were unrealistic as 46 μ_B/Mn and –2000 K, respectively. Above 60 K, magnetic susceptibility was difficult to be explained by the Curie-Weiss law, suggesting that $Y_2Mn_3Fe_9P_7$ is in an anomalous paramagnetic state.

Fig. 8 shows the density of states (DOS) and projected DOS (PDOS) of $Y_2Fe_{12}P_7$ and $Y_2Mn_3Fe_9P_7$ obtained from the calculation of the electronic band structure in a nonmagnetic (paramagnetic) state. Here, DOS is per formula unit, and PDOS is per the corresponding atom. PDOS of the tetrahedral site is the averaged value of the PDOS of the three tetrahedral sites. As shown in Fig. 8 (a), the DOS at the Fermi level (E_F) of $Y_2Mn_3Fe_9P_7$ is approximately twice that of $Y_2Fe_{12}P_7$. This enhancement of DOS at E_F seems caused by a shift of the entire DOS along the energy axis with the Mn substitution. Thus, the Mn substitution may dope holes to the conduction band. Actually, the Mn substitution leads to a shift in PDOS of the tetrahedral site as shown in Fig. 8 (b) and (c). However, for the pyramidal site, the band structure itself seems to change with the Mn substitution, and thus a simple rigid band model is not applicable to the pyramidal site. Although it is difficult to get information on the localized moment and its antiferromagnetic order from the band structure, the large PDOS at both the sites would relate to the magnetism in $Y_2Mn_3Fe_9P_7$.

4 Conclusion

In summary, we successfully synthesized polycrystalline samples of $Y_2(Mn_xFe_{1-x})_{12}P_7$ (x = 0–0.9). From the ^{57}Fe Mössbauer spectroscopy, we found that Mn atoms occupy the pyramidal sites selectively. An antiferromagnetic transition of $Y_2Mn_3Fe_9P_7$ is ascribed to the magnetic moments of the Mn atoms at the pyramidal site. The electronic band structure calculation showed large DOS at the Fermi level in $Y_2Mn_3Fe_9P_7$, suggesting enhanced electron correlation.

Acknowledgements

This work was supported by JSPS KAKENHI Grant Number JP20K05663.

References

1) Y. Kamihara, T. Watanabe, M. Hirano, H. Hosono: J. Am. Chem. Soc., **130** (2008) 3296-3297.
2) Y. Kamihara, H. Hiramatsu, M. Hirano, R. Kawamura, H. Yanagi, T. Kamiya, H. Hosono: J. Am. Chem. Soc., **128** (2006) 10012-10013.
3) T. Watanabe, H. Ynagi, T. Kamiya, Y. Kamihara, H. Hiramatsu, M. Hirano, H. Hosono: Inorg. Chem., **46** (2007) 7719-7721.
4) A. Pal, S. S. Mehdi, M. Husain, B. Gahtori: J. Appl. phys., **110** (2011) 103913-1-6.
5) K. Momma, F. Izumi: J. Appl. Crystallogr., **44**, (2011) 1272-1276.
6) W. Jeitschko, U. Meisen, E. J. Reinbold: Z. Anorg. Allg.

Chem., **638** (2012) 770-778.
7) H. Ohta, Y. Watanabe, A. Miyake, M. Tokunaga, H. Aruga. Katori: J. Jpn. Soc. Powder Powder Metallurgy, **63** (2016) 652-656.
8) H. Raffius, E Mörsen, B. D. Mosel, W. Müller-Warmuth, T. Hilbich: J. Phys. Chem. Solids, **52** (1991) 787-795.
9) K. Zeppenfeld, W. Jeitschko: J. Phys. Chem. Solids, **54** (1993) 1527-1531.
10) E. Dhahri: J. Phys.: Condens. Matter., **8** (1996) 4351-4360.
11) S. S. Stoyko, K. K. Ramachandran, C. S. Mullen, A. Mar: Inorg. Chem., **52** (2013) 1040-1046.
12) B. K. Srivastava, T. Ericsson, L. Höggström, H. R. Verma, Y. Andersson, S. Rundqvist: J. Phys. C: Solid State Phys., **20** (1987) 463-472.
13) Y. Kato, H. Ohta, H. Aruga Katori: Solid State Phenom., **289** (2019) 164-169.
14) F. Izumi, K. Momma: Solid State Phenom., **130** (2007) 15-20.
15) P. Blaha, K. Schwarz, G. Madsen, D. Kvasnicka, J. Luitz: WIEN2k, An Augmented Plane Wave Plus Local Orbitals Program for Calculating Crystal Properties (2014).
16) R. Fruchart, A. Roger, J. P. Senateur: J. Appl. Phys., **40** (1969) 1250-1257.
17) M. Reehuis, W. Jeitschko: J. Phys. Chem. Solids, **51** (1990) 961-968.